Int. J. Electrochem. Sci., 12 **(2017)** 8217 – 8226, doi: 10.20964/2017.09.37

International Journal of
ELECTROCHEMICAL
SCIENCE
www.electrochemsci.org

Controlled Synthesis of CuO from needle to flower-like Particle Morphologies for Highly Sensitive Glucose Detection

Xianguo Ma[1], *Qian Zhao*[2], *Hui Wang*[2,*] *and Shan Ji*[1,*]

[1] School of Chemical Engineering, Guizhou Institute of Technology, Guiyang, 550003, China,
[2] College of Chemistry and Chemical Engineering, Northwest Normal University, Lanzhou 730070, China
[*]E-mail: jissshan@126.com, wanghui3931@126.com

Received: 6 May 2017 / *Accepted:* 11 July 2017 / *Published:* 13 August 2017

CuO particles with morphologies ranging from "needle", "flat flowers" to "peony-like" flower shape were prepared by varying hydrothermal reaction times. The structure and morphology of the CuO samples were characterized by X-ray diffraction, BET and scanning electron microscopy, and these samples were evaluated as catalysts for glucose oxidation in alkaline solution. Of the three particle morphologies, peony-like CuO produced the highest glucose sensitivity of 1322 μA mM^{-1} cm^{-2}, with a broad detection range of 1.0 μM - 4.0 mM, and a detection limit of 0.5 μM under an applied potential of +0.5 V vs. Ag/AgCl. The peony-like CuO electrode also had excellent selectivity in the presence of interfering agents which usually co-exist in solution, for example uric acid, ascorbic acid and sodium chloride). Overall, we conclude that complex particle structure (of possible multiple grain boundary content) improves sensitivity for glucose detection and forms a target for developing effective non-enzymatic sensors.

Keywords: Copper oxide; Hierarchical structure; Glucose oxidation; Sensor.

1. INTRODUCTION

Sensing devices for rapid and accurate detection of glucose are required in areas of clinical diagnostics, biotechnology and food companies. In recent decades, various glucose biosensors based on the enzymatic catalyst, glucose oxidase, were developed. However, such sensors suffer from instability since glucose oxidase activity can be easily influenced by temperature, pH, chemicals and humidity [1, 2]. Enzyme-free detection of glucose is of growing interest due to advantages including their cheap, simple, fabrication and storage conditions, resistance to degradation (i.e. when compared to enzyme denaturation), greater stability toward changes in temperature and pH, and greater resistance

to toxic chemicals [3, 4]. Various enzyme-free glucose sensors based on nanomaterials such as metals[5, 6], metal alloys[4], and metal oxides[7-9] have shown promise. Particularly, transition metal oxides (e.g. ZnO[10], NiO[11], Fe_2O_3[12], MnO_2[13], RuO_2[14] and Co_3O_4[15]), are generally low in cost with high stability and high catalytic activity for glucose oxidation.

Recently, CuO has attracted attention due to its low toxicity, simple production, low cost, high electro-catalytic activity, and its promoting effect on electron transfer rate from the transition of its redox couple during glucose oxidation [3, 16, 17]. The electrochemical performance of nano-structured CuO highly is closely linked with particle size and morphologies [18]. Various CuO nanomaterials of different size and shape have been previously evaluated for their glucose oxidation activity, and these include spheres [19], needles [20], rods [21], wires [22], sheets [23], particles [24], flowers [25, 26], urchins [27, 28], platelets [29] and rods [29]. To date, however, a clear correlation between morphological type/complexity alone in relation glucose activity remains slightly ambiguous due to variations in other factors such as crystal polymorphs etc.

Herein, we synthesize simple to increasingly complex hierarchical monoclinic CuO particle structures and evaluate their respective activities in glucose detection. The most highly clustered particle form of CuO, which resembled dense peony-like flowers, produced the highest glucose oxidation activity compared to simple needle and flat flower-like morphologies. The possibility that an increased content of grain boundaries in more complex morphologies underlies high levels of glucose oxidation activity is therefore considered as reasonable explanation behind this observation.

2. EXPERIMENTAL

2.1 Material Synthesis

All chemicals used in this paper were of analytical grade and used without further purification. CuO particles were synthesized as follows: $CuCl_2$ (40 mg) was dissolved in 30 ml of ultrapure water, followed by addition of 3.6 mL $NH_3 \cdot H_2O$ (1 wt%) solution with stirring for 10 min to form a suspension. The slurry from the suspension was transferred into a Teflon-lined autoclave and heated at 200 ^oC for different hydrothermal dwell times (HDT), namely 10 min, 30 min or 120 min. After cooling to room temperature, the products were collected by filtration, washed with deionized water 5 times, and finally dried at 60 ^oC for overnight. The obtained products heated at 200 ^oC for 10 min, 30 min and 120 min were denoted as CuO1, CuO2 and CuO3 respectively.

2.2 Characterization

The crystalline structures of the samples were analyzed using X-ray diffraction (XRD) on a Shimadzu XD-3A (Japan) goniometer, using Cu Kα radiation operated at 40 kV and 35 mA). The morphologies of the samples were observed by a Carl Zeiss Ultra Plus field emission scanning electron microscope (SEM). Brunauer -Emmett-Teller (BET) specific surface area was calculated from the absorption branch of N_2 isotherm on Quantachrome Autosorb-1 volumetric analyzer.

2.3 Electrochemical measurements

Electrochemical measurements were carried out on an electrochemical work station (CHI 650D). A conventional three-electrode electrochemical cell was used comprising a platinum wire counter electrode, an Ag/AgCl (saturated KCl solution) reference electrode, and a working electrode comprising a thin film catalyst layer mounted on a 5-mm diameter glassy carbon disc. The thin film was prepared as follows: 2 mg of catalyst were dispersed ultrasonically in 0.6 mL of Nafion/ethanol (2.5 wt.% Nafion). 8 μL of the above solution was transferred onto the glassy carbon and then dried in the air.

3. RESULTS AND DISCUSSION

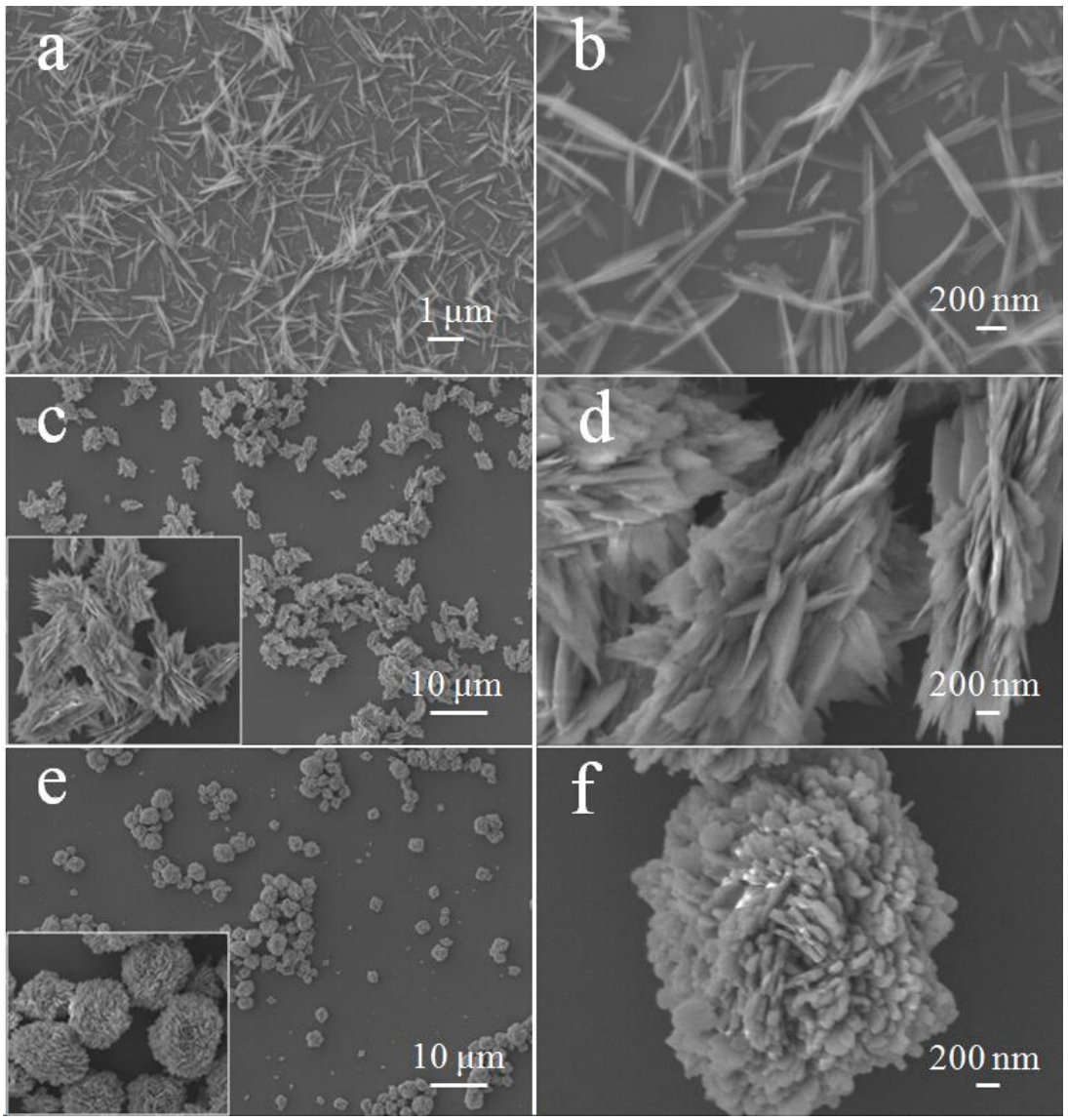

Figure 1. Increasing hierarchical complexity of CuO samples prepared with increasing HDT: SEM images (a,b) CuO1 (10-min HDT); (c,d) CuO2 (30-min HDT); and (e,f) CuO3 (2-h HDT).

Figure 1 shows SEM images of the as-prepared CuO samples under different magnification. CuO1 (Figure 1 a,b) formed uniform-sized simple needle-like particles of ~1.5 μm length and ~70 nm width. CuO2 (Figure 1 c) formed flat flower-like particle clusters (inset Figure 1 c), and the magnified SEM image of CuO2 (Figure 1 d) shows the clusters are formed of aggregated small sharply pointed sheets. Finally, CuO3 (Figure 1 e) possesses tighter clusters of smaller, more numerous, bluntly pointed sheets, that in aggregate have peony-like flower morphology (inset Figure 1 e, and 1 f). Therefore, increasing HDT clearly increased the hierarchical complexity of the particles.

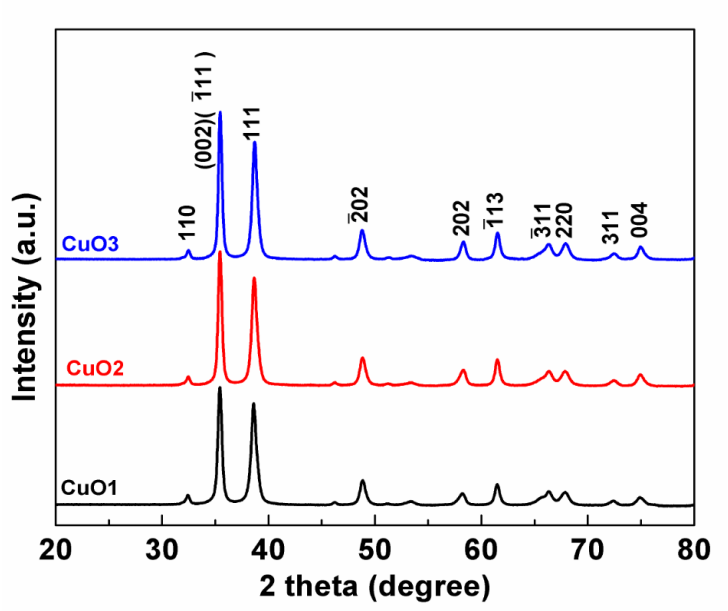

Figure 2. XRD patterns of the three CuO samples.

XRD analyses of the three CuO samples' crystal structures (Figure 2) revealed all three generated typical diffraction peaks of monoclinic phase CuO (JCPDS 48-1548), with no peaks correlating to $Cu(OH)_2$. Therefore, despite their very different morphologies, the particles appear to share the exact same pure phase crystal structure.

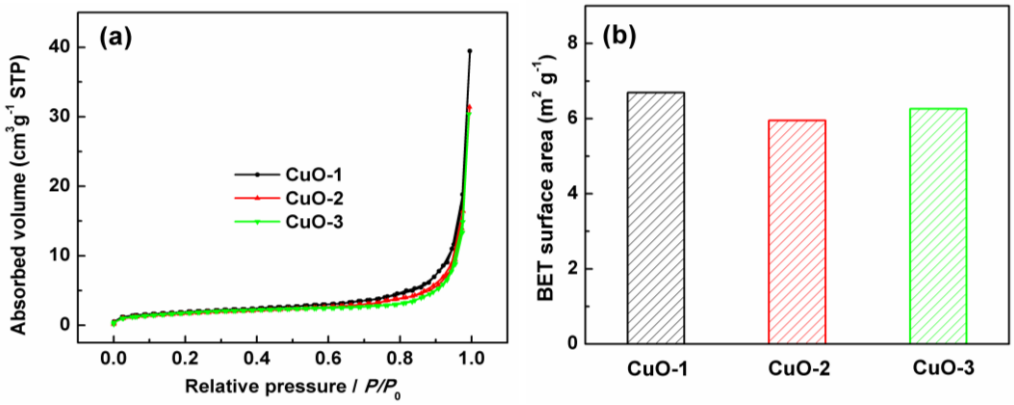

Figure 3. (a) N_2 isotherms and (b) BET surface area of CuO1, CuO2 and CuO3.

For the catalysts, the specific surface area is one of key factors resulting different catalytic performances. The BET surface area the as-prepared CuO1, CuO2, and CuO3 were characterised by the adsorption-desorption isotherms of N_2 at -196^oC and shown in Figure 3. As shown in Figure 3a, the isotherms of all three samples belong to type I in the IUPAC classification. At the low relative pressure region, there are not uptake in three isotherms, which indicates that no microporos existed in these three samples. With increasing the relative pressure, no hysteresis loop was observed, which means that these three samples don't contain mesoporous or macroporou structures. The N_2 isotherms of CuO1, CuO2 and CuO3 clearly show that the structures formed in these three samples are very dense without porous structures. Figure 3b shows the BET surface areas of CuO1, CuO2 and CuO3 are almost the same with each other, which is 6.7, 6.0 and 6.3 m^2g^{-1} respectively. The observations imply that the BET surface areas don't change when the structures of CuO1, CuO2 and CuO3 changed from needle-like particles to peony-like flower structure.

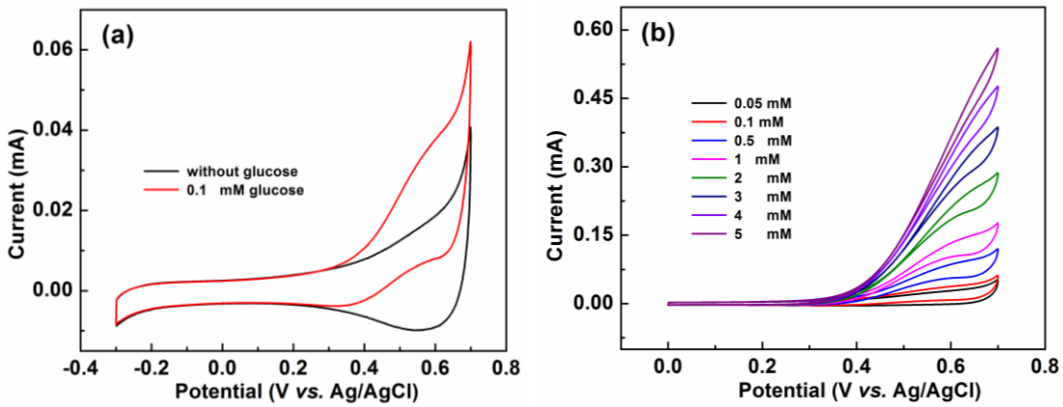

Figure 4. (a) CV curves of the CuO3 electrode in 0.1 M NaOH and 0.1 M NaOH + 0.1 mM glucose solution at scan rate of 50 mV s^{-1}; (b) CV curves of the CuO3 electrode in 0.1 M NaOH + 0.05~5 mM glucose solution at scan rate of 50 mV s^{-1}.

To evaluate the electrochemical behavior of the CuO samples, cyclic voltammetry (CVs) was carried out in 0.1 mol L^{-1} NaOH either in the presence or absence of glucose. Figure 4 a shows the CV curves of CuO3 in the absence and presence of 0.1 M glucose (black and red curves respectively). In the absence of glucose reversible redox activity occurred between 0.1 to 0.7 V, most likely arising from transition of Cu (II) and (III) oxidation states [18, 30]. Here, it is of interest to note that electron transfer between Cu (II) and Cu (III) may aid electron transfer during glucose oxidation. In the presence of 0.1 M glucose (Figure 4 a), a notable rise in oxidation current begins at 0.32 V in the positive scan direction, indicating that CuO3 catalyzed glucose oxidation [26, 28]. Figure 4 b shows that with increasing glucose concentration over a range of 0.05, 0.1, 0.5, 1, 2, 3, 4 and 5 mM, the activity of CuO3 increased correlatively, which indicates specific electrocatalytic activity toward glucose oxidation had occurred.

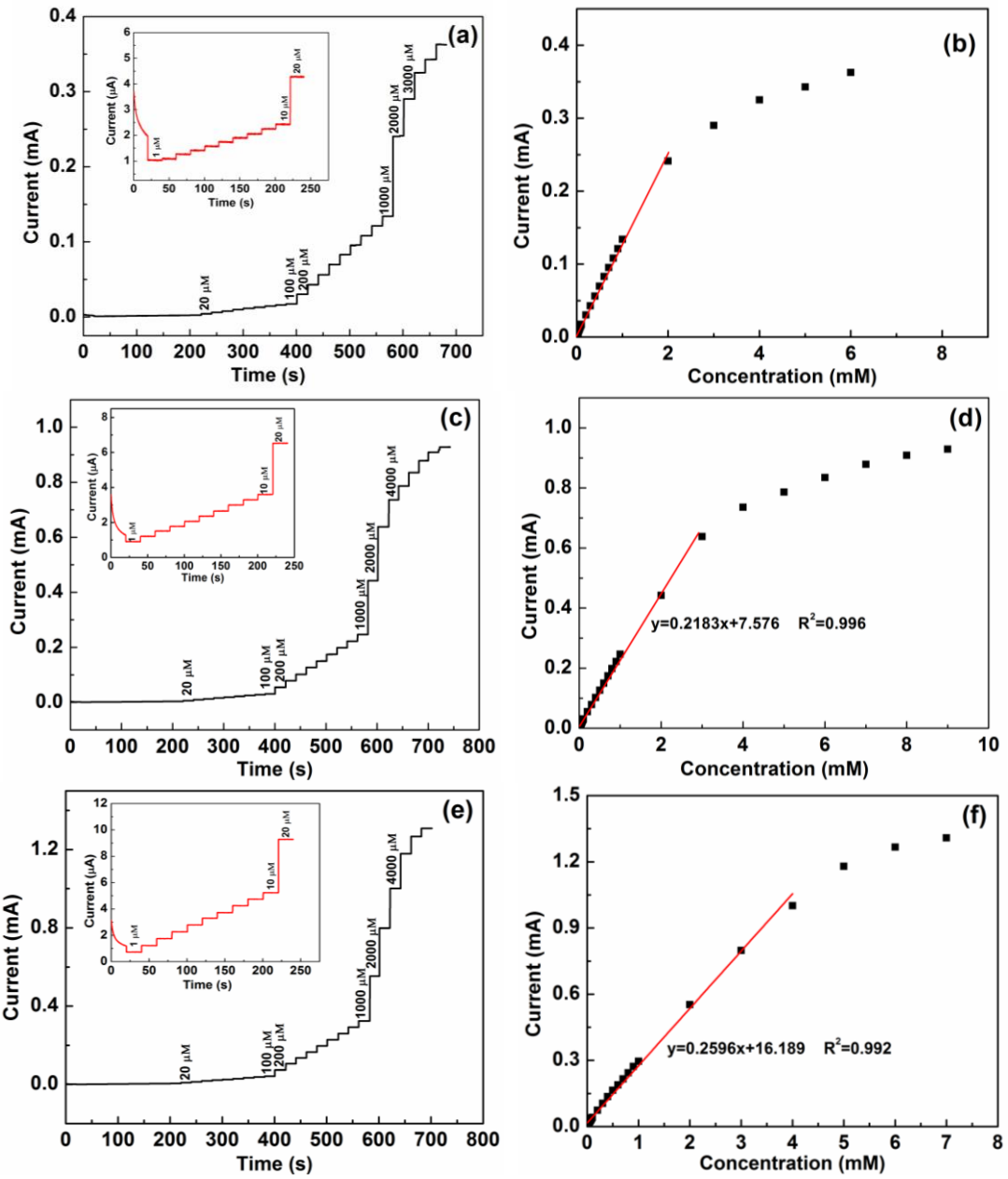

Figure 5. Amperometric response of CuO1 (a-b), CuO2 (c-d), and CuO3 (e-f) electrodes with increasing glucose concentration in 0.1 M NaOH at an optimal detection potential of +0.5 V vs. Ag/AgCl. Insets show enlarged areas of the amperometric response curves at low glucose concentration (1 to 20 μM). The current–glucose concentration calibration curves (b, d, f) for CuO1, CuO2, and CuO3 respectively are shown on the right hand side of the figure.

Amperometric evaluation of the CuO samples' activities for glucose oxidation (Figure 5) offered a sensitive detection system of low signal-to-noise ratio. The method provides effective mixing of the sample solution resulting in high convective mass transport to the electrode surface and thus allows rapid detection of an analyte. The response of the CuO electrodes was studied using successive injections of glucose to the 0.1 M NaOH solution under an optimized detection potential at +0.5 V. For the overall concentration range (1 to 4000 μM), increasing current response can be clearly seen in the

order of CuO1 < CuO2 < CuO3, and the insets of Figures 5 (a, c and e) show this pattern is maintained at low glucose concentrations of 1 to 20 μM. The calibration curves (Figure 5 b, d and f) show the three sensors produced a linear response to glucose concentration, and the corresponding linear fit equations with the correlation coefficient (R^2) are shown in the Figures. From the calibration curves, sensitivity values at a signal/noise ratio of 3, and ranges were obtained as listed in Table 1. The limits of detection (LOD) of the sensors were estimated using the following equation [26, 31]:

$$\mathrm{LOD} = \frac{3s_b}{m}$$

where m is the slope value of the calibration plot and s_b is the deviation got from 10 different measurements of the blank signal. LOD was calculated to be 1.7, 1.3 and 0.5 μM for CuO1, CuO2 and CuO3. Therefore, based on the above results, CuO3 has the highest sensitivity, maximum linear range, and lowest LOD among the three CuO samples.

It is well-known that the electrocatalytic properties are closely linked with crystal structure, composition, specific surface areas and morphologies. The XRD results show that the crystal structures of these three CuO samples are the same, and BET observations found that there isn't porous structure existed in these three CuO samples. Therefore, the catalytic differences of CuO1, CuO2 and CuO3 should result from their various morphologies. There are numorous nanoheets in CuO3, along which numerous grain boundaries could exist. Grain boundaries between crystalline phases of a catalyst are proposed to act as the catalytically active sites [32-34]. Therefore, the highly hierarchical structure of CuO3 may provide many grain boundaries acting as catalytic active sites for the glucose oxidation resulting in its high sensitivity in glucose detection.

Table 1. Comparison of key performance for reported CuO-based electrodes in glucose detection.

Electrode	Detection potential/V vs. Ag/AgCl	Sensitivity/ μA cm^{-2} mM^{-1}	Linear range/ mM	LOD / μM	Reference
CuO1	0.5	637	0.001-2	1.7	This work
CuO2	0.5	1112	0.001-3	1.3	
CuO3	0.5	1322	0.001-4	0.5	
CuO nanowires/Cu	0.35	2217.4	0.001-18.8	0.3	[16]
CuO nanourchins	0.57	1634	0.01-5	1.97	[28]
CuO nanowires	0.55	648.2	---	2	[21]
CuO nanowires/Cu	0.33	490	0.0004-2	0.049	[22]
CuO nanofibers	0.40[a]	431.3	0.006-2.5	0.8	[35]
CuO nanoflowers	0.5	2657	0.01-5	1.71	[25]
Dandelion-like CuO films	0.60[a]	5368	0.005-1.6	1.2	[26]

a: SCE reference electrode.

Table 1 shows the position of peony-like CuO3 activity in relation to previously reported CuO glucose sensors. The sensitivity and detection limit of CuO3 are comparable and better than those obtained by [21, 22, 35], which have simple nanowire/fibre morphology, but less than those of [16, 25, 26, 28], all of which have complex particle morphologies, with the exception of [16] which has mixed CuO/Cu composition. Therefore, considering the pure CuO samples in Table 1, the complex structure of peony-like CuO3 along with the complex morphologies of [25, 26 and 28], are most likely to have numerous grain boundaries that produce high levels of glucose oxidation activity.

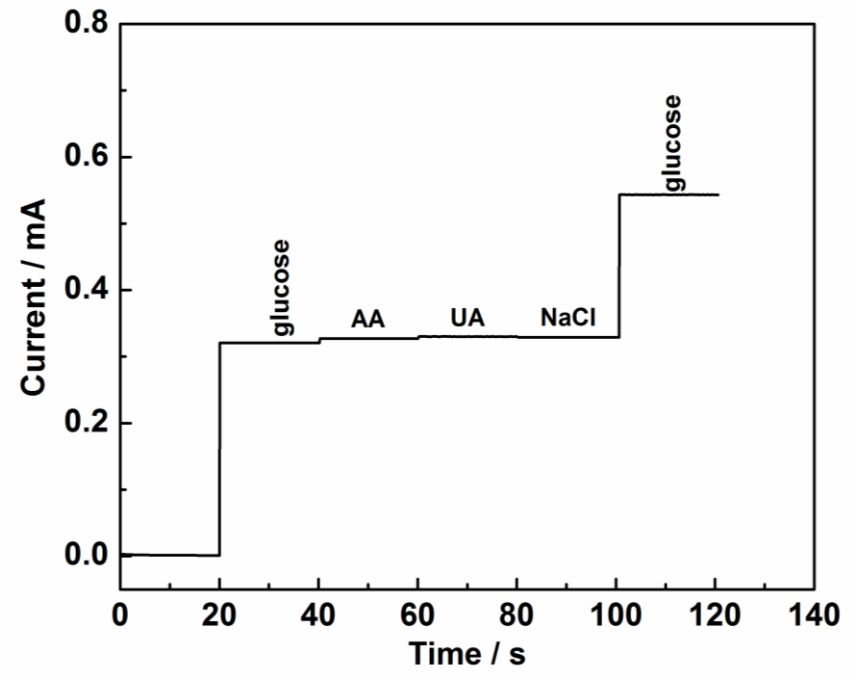

Figure 6. Amperometric response of CuO3 with continuous injections of 1.0 mM glucose showing minimal interference from 0.1 mM of AA, UA, and NaCl in 0.1 M NaOH at a potential of +0.5 V vs. Ag/AgCl.

Some oxidative species such as ascorbic acid (AA), uric acid (UA), NaCl and carbohydrate compounds, which usually exist with glucose in the samples and consequently interfere with glucose detection. Therefore, selectivity for glucose is an important factor in the use of glucose biosensors. Normal physiological levels of glucose range between 3-8 mM and are least 10 times higher than that of commonly occurring interfering species. Figure 6 shows the amperometric response of CuO3 to stepwise addition of 1.0 mM glucose with 0.1 mM AA, UA and NaCl at an applied potential of +0.5 V. As can be seen, an obvious glucose oxidative response occurred with no obvious current response for these species. Therefore, high selectivity for glucose was achieved on CuO3 in alkaline media. In the alkaline environment, the CuO would be negatively charged on its surface. Meanwhile, interfering species such as UA and AA are also negatively charged because of the deprotonating effect in alkaline solution [24, 26, 27, 29], and therefore would be repelled by the negatively charged CuO3, showing correspondingly low signals.

4. CONCLUSIONS

Monoclinic phase CuO particles of increasing morphological complexity (comprising needles, flat flowers, and peony-like flowers) were prepared through increasing hydrothermal dwell times (HDT). The most complex, peony-like particles, (denoted herein as CuO3) could detect the lowest glucose levels (0.5 μM) and had the highest sensitivity (1322 μA mM^{-1} cm^{-2}) with with broad detection range of 1.0 μM–4.0 mM. The high activity of CuO3 may correlate to it containing more catalytically active sites for glucose oxidation on the many grain boundaries within its highly clustered makeup of nanosheets. Furthermore, the CuO3 electrode also showed high selectivity for glucose oxidation in the presence of interfering species ascorbic acid (AA) and uric acid (UA). We conclude that increased hierarchical structure, achieved via increased HDT, results in improved glucose oxidation/detection, which possibly results from particle morphology of increased grain boundary content. Overall, the combination of high sensitivity and selectivity makes the CuO3 electrode a promising non-enzymatic glucose biosensor.

ACKNOWLEDGEMENT
The authors would like to thank the National Natural Science Foundation of China (No. 51603049) and Natural Science Foundation of Guizhou Province (No. qian ke he J zi [2015]2059) for financially supporting this work.

References

1. Z. Shahnavaz, P.M. Woi, Y. Alias, *Ceramics International*, 41 (2015) 12710-12716.
2. Z. Yu, H. Li, X. Zhang, N. Liu, W. Tan, L. Zhang, *Biosensors & bioelectronics*, 75 (2016) 161-165.
3. M.-J. Song, S.-K. Lee, J.-H. Kim, D.-S. Lim, *Journal of the Electrochemical Society,* 160 (2013) B43-B46.
4. Y. Miao, J. Wu, S. Zhou, Z. Yang, R. Ouyang, *Journal of the Electrochemical Society,* 160 (2013) B47-B53.
5. P. Sivasakthi, G.N. Ramesh Bapu, M. Chandrasekaran, *Materials science & engineering. C, Materials for biological applications,* 58 (2016) 782-789.
6. E. Mijowska, M. Onyszko, K. Urbas, M. Aleksandrzak, X. Shi, D. Moszyński, K. Penkala, J. Podolski, M. El Fray, *Applied Surface Science,* 355 (2015) 587-592.
7. H. Li, J. Li, D. Chen, Y. Qiu, W. Wang, *Sensors and Actuators B: Chemical*, 220 (2015) 441-447.
8. T. Bordjiba, D. Bélanger, *Electrochimica Acta*, 55 (2010) 3428-3433.
9. C. Karuppiah, M. Velmurugan, S.-M. Chen, S.-H. Tsai, B.-S. Lou, M. Ajmal Ali, F.M.A. Al-Hemaid, *Sensors and Actuators B: Chemical*, 221 (2015) 1299-1306.
10. K. Singh, A. Umar, A. Kumar, G.R. Chaudhary, S. Singh, S.K. Mehta, *Science of Advanced Materials*, 4 (2012) 994-1000.
11. V. Veeramani, R. Madhu, S.-M. Chen, P. Veerakumar, C.-T. Hung, S.-B. Liu, *Sensors and Actuators B: Chemical*, 221 (2015) 1384-1390.
12. X. Cao, N. Wang, *Analyst,* 136 (2011) 4241-4246.
13. S. Yang, L. Liu, G. Wang, G. Li, D. Deng, L. Qu, *Journal of Electroanalytical Chemistry,* 755 (2015) 15-21.
14. R.M. Tehrani, S. Ab Ghani, *Biosensors & bioelectronics,* 38 (2012) 278-283.
15. C. Guo, X. Zhang, H. Huo, C. Xu, X. Han, *Analyst,* 138 (2013) 6727-6731.

16. Z. Li, Y. Chen, Y. Xin, Z. Zhang, *Scientific reports*, 5 (2015) 16115.
17. W. Wang, L. Zhang, S. Tong, X. Li, W. Song, *Biosensors & bioelectronics*, 25 (2009) 708-714.
18. Y. Ma, H. Wang, K. Julian, S. Ji, W. Lv, R. Wang, *Journal of Power Sources*, 300 (2015) 344-350.
19. E. Reitz, W. Jia, M. Gentile, Y. Wang, Y. Lei, *Electroanalysis*, 20 (2008) 2482-2486.
20. D. Ye, G. Liang, H. Li, J. Luo, S. Zhang, H. Chen, J. Kong, *Talanta*, 116 (2013) 223-230.
21. X. Wang, C. Hu, H. Liu, G. Du, X. He, Y. Xi, *Sensors and Actuators B: Chemical*, 144 (2010) 220-225.
22. Z. Zhuang, X. Su, H. Yuan, Q. Sun, D. Xiao, M.M.F. Choi, *The Analyst*, 133 (2008) 126-132.
23. Z. Ibupoto, K. Khun, V. Beni, X. Liu, M. Willander, *Sensors*, 13 (2013) 7926-7938.
24. R. Ahmad, M. Vaseem, N. Tripathy, Y.-B. Hahn, *Analytical Chemistry*, 85 (2013) 10448-10454.
25. S. Sun, X. Zhang, Y. Sun, S. Yang, X. Song, Z. Yang, *Physical Chemistry Chemical Physics*, 15 (2013) 10904.
26. K. Li, G. Fan, L. Yang, F. Li, *Sensors and Actuators B: Chemical*, 199 (2014) 175-182.
27. S. Sun, X. Zhang, Y. Sun, S. Yang, X. Song, Z. Yang, *ACS applied materials & interfaces*, 5 (2013) 4429-4437.
28. S. Sun, X. Zhang, Y. Sun, J. Zhang, S. Yang, X. Song, Z. Yang, *RSC Advances*, 3 (2013) 13712-13719.
29. F. Huang, Y. Zhong, J. Chen, S. Li, Y. Li, F. Wang, S. Feng, *Analytical Methods*, 5 (2013) 3050.
30. Y. Ma, H. Li, R. Wang, H. Wang, W. Lv, S. Ji, *Journal of Power Sources*, 289 (2015) 22-25.
31. J. Yang, M. Cho, Y. Lee, *Biosensors & bioelectronics*, 75 (2015) 15-22.
32. F. Maillard, S. Schreier, M. Hanzlik, E.R. Savinova, S. Weinkaufb, U. Stimminga *Phys Chem Chem Phys*, 7 (2005) 385-393.
33. J. Zhang, Y. Xu, B. Zhang, *Chemical Communications*, 50 (2014) 13451-13453.
34. H. Wang, Z. Liu, Y. Ma, K. Julian, S. Ji, V. Linkov, R. Wang, *Physical Chemistry Chemical Physics*, 15 (2013) 13999-14005.
35. W. Wang, L. Zhang, S. Tong, X. Li, W. Song, *Biosens. Bioelectron.* , 25 (2009) 708-714.

© 2017 The Authors. Published by ESG (www.electrochemsci.org). This article is an open access article distributed under the terms and conditions of the Creative Commons Attribution license (http://creativecommons.org/licenses/by/4.0/).